ISSN: 0974-5823 Vol. 7 (Special Issue, Jan.-Feb. 2022)

International Journal of Mechanical Engineering

Microstructure and Mechanical Properties of Additive Manufactured IN718 Alloy after Heat-Treatment

Ajay Kumar Maurya[1*], Amit Kumar[2]

[1,2]Department of Mechanical Engineering, National Institute of Technology Patna, Bihar 800005, India.

*Correspondence

Abstract: Inconel is a very demanding material and is mostly used in the aerospace industry to make rocket engine parts due to its excellent mechanical properties. Sometimes very complicated structures are required which is very difficult to make parts by conventional methods. Additive manufacturing techniques can fabricate complex parts more easily than conventional methods but it has not been tested yet. So, it is necessary to examine the mechanical and microstructural properties of additive-made components. In this paper Inconel 718 alloy samples were made using additive manufacturing powder-bed-fusion based direct metal laser sintering process. Mechanical properties were examined after heat treatment. It was observed that the yield strength and tensile strength were higher for direct aged heat-treated samples fabricated in the horizontal direction. Fractography and microstructural properties were examined using scanning electron microscopy, and XRD analysis was conducted for phase identification.

Keywords: Additive Manufacturing, Inconel 718 Alloy, Microstructure, Mechanical Properties

1. Introduction

Additive manufacturing (AM) technology is an easy means of manufacturing complex three-dimensional designs and utilizes less material than traditional manufacturing methods. It is defined as manufacturing components from 3D CAD models by layering material with a layer thickness as small as 20 µm [1]. The AM technique has various advantages over the traditional manufacturing of industrial components, including design freedom, higher productivity, and less material and energy waste [1]. Parts made in AM are employed in various applications, including medical devices, aerospace, automotive, and power industries [2].

Inconel 718 alloy is used in many applications due to its excellent qualities such as good tensile, and comprehensive stress, outstanding weldability, easy processing, and relatively low cost. These materials are extensively used in nuclear and petrochemical industries, aerospace engines, and gas turbines. The primary casting process for manufacturing complex superalloy components is investment casting [3]. However, the related solidification defects, such as dendritic segregation, microporosity, and the formation of δ and Laves phases, have harmful effects on the mechanical properties of the cast superalloy [4]. To address this problem, hot isostatic pressing is required to close pores, and heat treatment to homogenize the microstructure, and improve the mechanical properties of the cast Inconel 718 superalloy.

Many studies have recently focused on the application of AM to the alloy Inconel 718. Dinda et al. [5] investigated the microstructural morphology of deposits produced using a CO_2 laser beam and metal powders and demonstrated that the microstructure and laser beam scanning patterns were correlated. Furthermore, changes in the hardness were related to the aging temperature difference. Dinda et al. [6] found that the grain structures were transformed entirely from columnar to homogenized equiaxed structures by increasing the annealing temperature from 1000 ^{0}C to 1100 ^{0}C and 1200 ^{0}C. However, as the annealing temperature increased, the material softened, and a decrease in hardness was observed for both AM produced IN625 and IN718. Zhu et al. [7] studied the changes and the strength of the deposit's microstructure resulting from manufacturing using a fiber laser and metal powder. This study related the grain size, dendrites, and Laves phases to the laser power and beam diameter. A tensile test was conducted on the deposits produced under various process conditions. Chen et al. [8] identified the process parameters that affect the cooling rate of deposits using a disc laser and metal powder. The microstructure and the hardness changed due to the separation of chemical components. Empirical formulae related to process parameters were applied to evaluate shape-related formation qualities, including deposit width and height, cooling rate, and hardness. Huang et al. [9] employed a homogenization heat treatment at 1066 ^{0}C for cast Inconel 718 to minimize boron (B) segregation at grain boundaries, which improved HAZ micro-fissuring resistance while lowering the volume percentage of NbC and laves. They discovered that the duration of cooling influences phases and elemental segregation, changing their mechanical properties. Microstructure & mechanical properties of SLM, cast, and forged IN718 were compared by Trosch et al. [10]. They discovered that at room temperature and 450 ^{0}C, the tensile mechanical characteristics of SLM IN718 samples were better than those produced by traditional methods. Ni et al. [11] reported the effect of heat-treatment on precipitation growth and mechanical properties of SLM IN718. And analyzed how heat treatment affected metallurgical properties such as grain growth and element segregation at grain boundaries. Other researchers have noted the presence of columnar grains with tiny dendritic features in the SLM as-printed IN718 [12]. Typical heat treatment does not entirely remove grain texture and dendritic segregation [13]. Still, the ageing heat treatment significantly increased the strength, characteristic of IN718 that goes through precipitation hardening. Rising the annealing temperature to 1160 ^{0}C for 4 hours, somewhat affected the grain structures of the parent γ phase, although dendritic segregation remained [14].

The mechanical performance is affected by the specific orientation in which the material is deposited in the SLM process since the anisotropy of the material depends on the building orientation [15]. Sun et al. [16,17] investigated the effects of structural orientation on the microstructure of CoCrMo alloy and IN718 alloy rods. The results reveal that the crystal orientation in the cylindrical axis may be adjusted by changing the build direction. Smith et al. [18] analyzed the microstructure and mechanical properties of the DMLS built Inconel 718 part considering the building orientation effect. Because of anisotropy, they discovered a nearly 7% difference in strength (tensile and compressive) between horizontally and vertically built samples. Amato et al. [19] investigated the tensile properties and hardness of DMLS produced Inconel 718 and analyzed hot isostatically pressed and heat-treated microstructural features in as-built samples. They reported that mechanical properties and crystallographic orientation could largely depend on building orientation and post-processing treatment. Deng et al. [20] investigated SLM's orientation dependence mechanical properties fabricated in IN718, but their findings were limited to vertical and horizontal directions.

From the available literature, many aspects of SLM manufactured in IN718 have been investigated but no extensive study has been made to illustrate the significant effect of industrial heat-treatment and build direction on microstructure and mechanical properties. Thus, the present study aims to analyze heat-treatment and building orientation-dependent mechanical and microstructural behavior of IN718 alloy build using the DMLS process in three building orientations.

2. Experimental Procedure and Methods

2.1 Materials

For the experimentation, IN718 alloy powder prepared by gas atomization was utilized. The used Inconel 718 powder's chemical composition is shown in Table 1.

Table 1. Weight % of IN718 alloy powder used.

Element	Ni	Cr	Nb	Mo	Ti	Al	Co	Cu	C	Fe
Wt. (%) Max/min	55/50	21/17	5.5/4.75	3.3/2.8	1.15/0.65	0.80/0.20	≤1.0	≤0.3	≤0.08	Bal

2.2 Powder characterization

The SEM image of the used powder is shown in Fig 1 (a), and the size morphology of one atom is shown in Fig. 1 (b). The SEM image was analyzed with ImageJ software, it was observed that the size of powder particles is in the range of 15 µm to 45 µm. From the SEM images, it can be seen that the shape and size of particles vary from atom to atom. Very tiny atoms were observed attached to the bigger-sized power particles some pore was also observed on some atom's surface. The powder has good flowability because the powder particles almost have a regular shape.

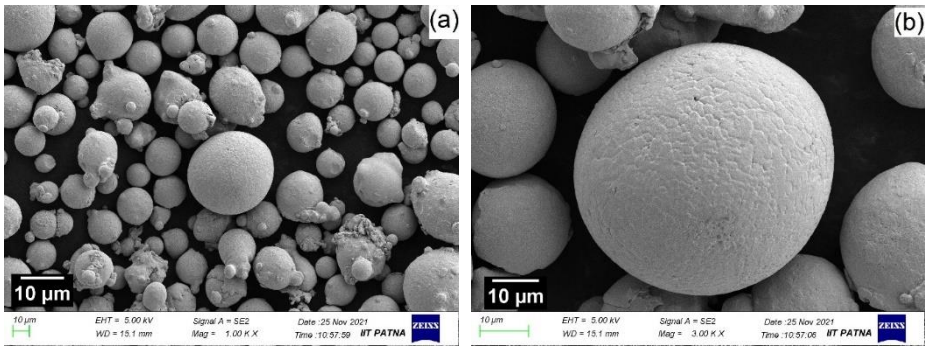

Fig. 1. (a) Powder particles used, and (b) a view of one tiny powder particle

2.3 Sample designing

The dog bone type tensile sample was modeled according to the ASTM standard E8 16a. The size of the tensile sample is 25.0 mm in gauge length, 2.0 mm in thickness, and 6.0 mm in gauge width as shown in Fig. 2.

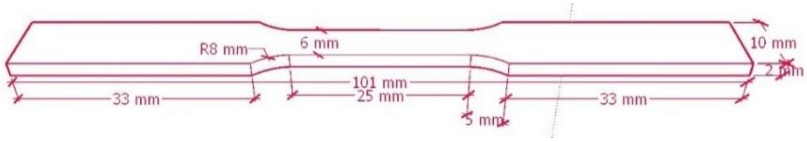

Fig. 2 Showing the modeled sample of a tensile specimen

2.4 Scan Strategy

For fabrication samples, a bidirectional scanning strategy was used to form layers with a 90^0 rotation after each layer as shown in Fig. 3.

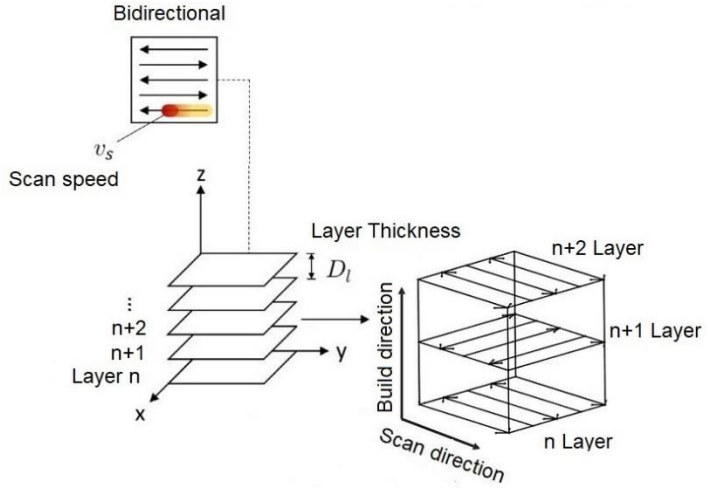

Fig. 3 Bidirectional scan strategy

2.5 Manufacturing of Test Pieces

The dog-bone miniature-sized tensile samples were fabricated as per design using an EOSINT M280 DMLS AM system that is available at the central tool room and training center, Bhubaneswar, India. (The details about machine specifications are given below in table 2, and the process parameters used for sample fabrication are given in table 3). The substrate was initially heated to 80 ^{0}C before starting the sample fabrication process. To keep contaminants out of the building chamber, the building chamber was shut, and the oxygen content inside the chamber was controlled. The excellent quality argon gas was continually injected inside the building area and allowed to flow over the built zone to keep the oxygen concentration below 0.1 percent to avoid phase transitions. The EOS proposed industry-standard process parameters were used. The sample was built in three building orientations (horizontally "0^0/H", inclined "45^0/D", and vertically "90^0/V"). After fabrication, samples were removed from the building chamber and separated from the substrate with the help of a wire-electro discharge machining.

Table 2. Machine specification

Parameter	Laser type	Laser power	Laser diameter	Scan speed	Wave-length (nm)	Build area (mm^3)
Value	Ytterbium fiber laser	400_{max} (W)	100-500	7000_{max} (mm/s)	1060-1100	250×250×325

Table 3. The parameters used for sample fabrication

Parameter	Laser type	Laser power	Scan speed	Layer thickness	Hatch spacing
Value	Ytterbium fiber laser	285 (W)	960 (mm/s)	40 (µm)	0.11 (mm)

2.6 Heat Treatment

A horizontal tube furnace is used to perform heat treatment as a post-process activity. The following thermal treatments are applied to as-built (AB) specimens: Homogenization (HSA) performed by heating with 10 ^{0}C per min rate until 1080 ^{0}C for 1 h followed by Furnace cooling, Solution treatment (SA) it consists of heating with 10 ^{0}C per min rate until 960 ^{0}C for 1 h followed by furnace cooling, & Ageing (DA) it consists of heating with 10 ^{0}C per min rate until 720 ^{0}C for 8 h followed 620 ^{0}C for 8 h by furnace cooling and air cooling respectively, considering industrial standard heat treatment for casting Inconel 718 alloy [12^{p4}]. After the heat treatments, three conditions of Inconel 718 were obtained HSA, SA, and DA.

2.7 Tensile Test

The tensile experiments were done in an open environment at room temperature using the universal testing machine (UTM) at a 0.5 mm/min strain rate (UTM specifications: Zwick Roell 250 kN load capacity available at the National Institute of Technology Patna).

2.8 X-Ray Diffraction

X-ray diffractometer with 45 kV and 35 mA, CuKa radiation was used to analyze the phases of samples before and after heat treatment. The scan range (2θ), ranging from 30^0 to 70^0 was selected to capture as many diffraction peaks as possible.

2.9 Microstructural Analysis

The Carl Zeiss EVO 50 SEM was also used to analyze the fracture surface morphology. The fabricated and heat-treated samples were ground using grit size 400 to 2500 and polished with a polishing cloth for metallographic investigation. An etchant quantity of 1.5 ml 30% H_2O_2 and 10 ml of hydrochloric acid was used for a few seconds to reveal the microstructure and strengthening phases.

3. Results and Discussion

3.1 Mechanical properties

Fig. 4 depicts and compares the tensile characteristics of the Inconel 718 alloy, considering the heat treatments and building orientation. These findings show that heat treatment enhances yield strength (YS) and Ultimate tensile strength (UTS), while

significantly reducing elongation at failure. The lack of γ'/γ" strengthening phases that would emerge after DA treatment might explain the comparatively low tensile strength in the AB state. Compared to heat-treated conditions, the direct ageing treatment produces the highest tensile strength but the lowest ductility. The solution annealing treatment produces lower ductility but slightly higher tensile strength compared to homogenization solution ageing treatment and comparable tensile characteristics [20].

The dependence of the built direction on the tensile properties is also examined. In H-built samples, YS and UTS are higher than that of D and V-built samples, but ductility is the reverse. When comparing the difference in tensile strength between V-built and H-built samples in each heat treatment condition, the difference reduces as the HT temperature and duration are increased. It may be noted that the defects of all samples are pretty minor, implying that this consistent difference is less likely to be caused by defects.

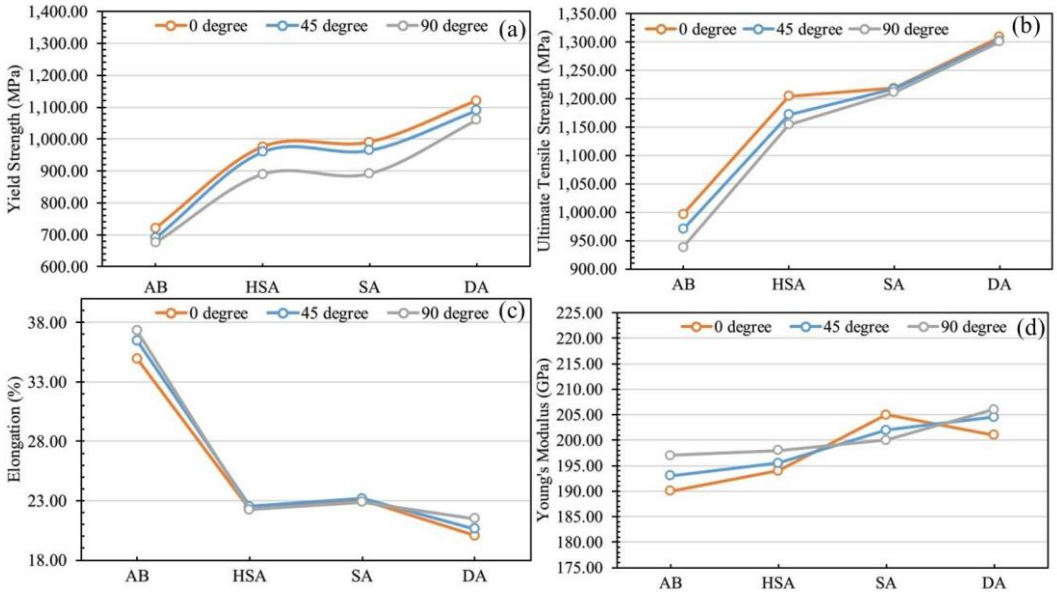

Fig. 4. Mechanical Properties: (a) σ0.2 YS, (b) ultimate tensile strength, (c) elongation at failure, (d) Young's modulus.

The tensile behavior of IN718 manufactured using SLM was studied by Wang et al. [12]. As-fabricated tensile findings for material aligned with the construction direction fell above and below those given here in the study. This is because, during solidification, the metastable Laves phase formed, which restricts the ductility of wrought Inconel 718 at room temperature [21]. According to Kirka et al. [22], only the last few layers of the build are expected to have Laves phase. Its influence on the mechanical characteristics of EBM Inconel 718 may be regarded as insignificant.

The mechanical properties reported in this study are nearly the same or higher as those reported in the literature [20]. The tensile behavior of the material was observed in the H, D, and V-built, it was discovered that post-processing heat-treatment applied to Inconel 718 alloy in this investigation was advantageous over that of as-fabricated material. The yield strength is nearly similar in post-processed tensile properties, and elongation at failure is higher than reported here. However, compared to the AMS cast Inconel to DMLS produced IN718, the DMLS produced samples observed higher tensile strength. Also, DMLS-produced Inconel shows better ductile behavior than wrought Inconel 718. This is primarily due to the occurrence of porosity aligned with the grain boundaries. However, comparing the outcomes of mechanical properties described in the literature is challenging because each is manufactured under different conditions and subjected to distinct HT processes. Wrought (W) values were derived from [23] for a material in a comparable state, which was a hot rolled bar that had been solution and double-aged according to AMS 5663.

3.2 Microstructural changes

Fig. 5 depicts the microstructural development resulting from various heat treatments. Performing the SA treatment, the melt pool borders and cellular-dendritic microstructure almost vanish, as shown in Fig. 5 (c). Furthermore, the low ageing temperature is not able to homogenize the segregation and dissolve the Laves phase; it retains its original size and shapes like an as-built state, as shown in Fig. 5 (e). Laves phases essentially disintegrate when the size drops significantly, and a substantial number of needle-like phases precipitate, both intergranular and intragranular. When the heat treatment temperature is increased to 1080 ^{0}C, Laves is dissolved further, as shown in Fig. 5 (a), though not entirely, since the cores of Laves phases remain inside microstructure. After homogenization, Laves released Nb and equally distributed it in the matrix than the SA. Under these conditions, application of solution treatment after homogenization will result in a δ precipitate near the grain boundaries. Equivalent results were also observed by Qi et al. [24] due to STA treatment. They observed a mass alteration of Laves into globular δ. Solution annealing of Inconel 718 manufactured by SLM at temperatures exceeding 1040 ^{0}C led to recrystallization, according to Chlebus et al. [14] performed solution annealed treatment (>960 ^{0}C) on Inconel 718 alloy fabricated with SLM. Consequently, the distinctive columnar grains were retained, with the addition of acicular delta precipitation near grain boundaries.

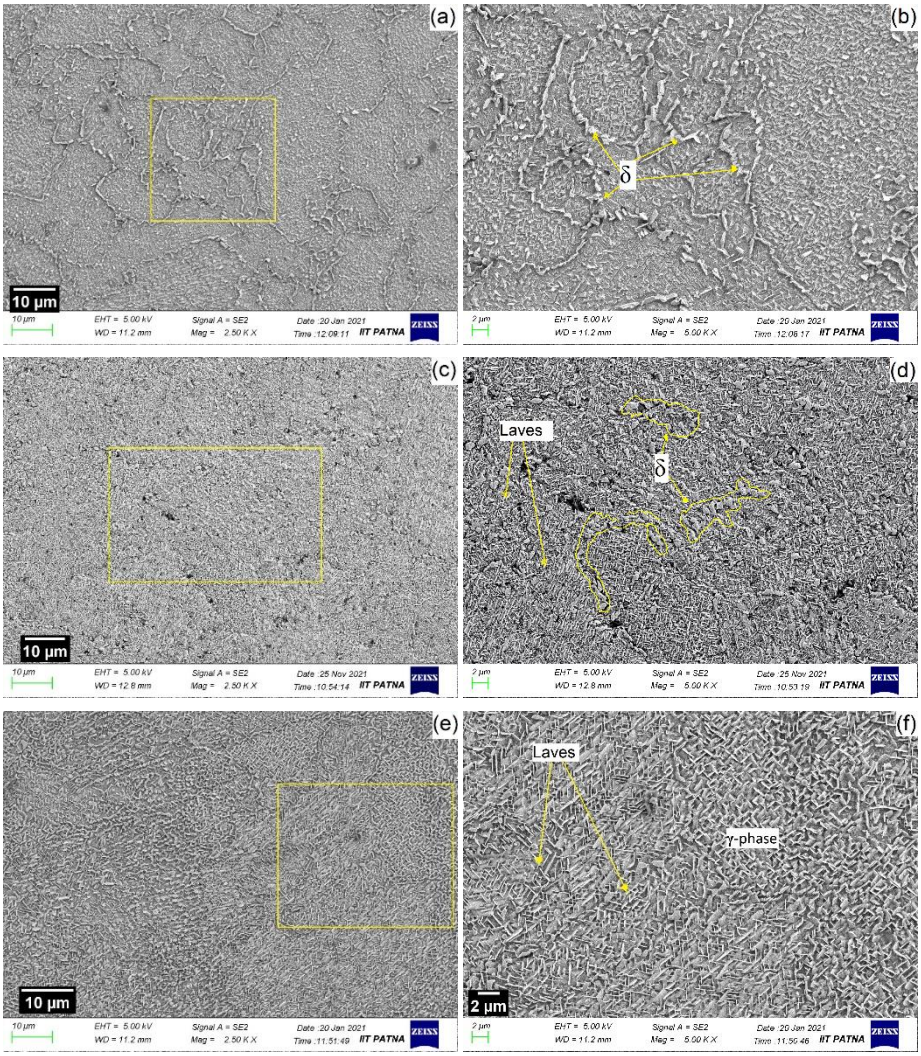

Fig. 5. Post-heat-treatment microstructure of an etched H-built sample: (a) HSA, (c) SA, and (e) DA, and the enlarged portions are shown in (b-d-f).

3.3 Phase Analysis using XRD

The XRD patterns before and after heat treatment are shown in Fig. 6. The XRD graph illustrates different peaks γ, δ, etc. γ, γ', and γ" peaks can hardly be distinguished as it overlaps in the XRD pattern because in the γ matrix, γ'/γ" precipitates are coherent. As TiC nanoparticles are modest in size and quantity compared to the γ matrix, they are challenging to detect in XRD. The peaks of the phases γ (2θ=44) are identified as higher for DA, but low peaks are present in the HSA/SA sample, which may be due to its smaller volume portion. In most cases, XRD does not detect phases present in less than 5% of the samples, so δ phases are not well identified. The Laves phase diffraction peaks are likewise not visible in the AB and HT samples. Therefore, SEM was needed to identify whether Laves phases and δ existed in HSA, SA, and DA samples, as shown in Fig. 5.

The peak point was marginally moved towards the higher 2θ value after the post-heat treatment, as illustrated in Fig. 6 (b). According to Bragg's law, the lateral shift of the diffraction peak is evidence of the dissolving process of the precipitate created during printing. i.e., heavy element diffusion into the matrix, such as titanium, molybdenum, and niobium. The diffraction peaks moved to higher 2θ values for the DA sample, implying a gradual removal of heavy components from the γ matrix. As a result, secondary phases progressively re-precipitate. When comparing the SA/HSA sample to the DA condition, the diffraction peaks appear to be moved farther towards a higher 2θ value, indicating more precipitation.

The volume proportion of each phase in the HT samples is challenging to determine γ, γ', and γ" phases because of the overlapping peaks. Due to their low content, additional minor phases such as Laves, δ, and carbides are ignored in the process.

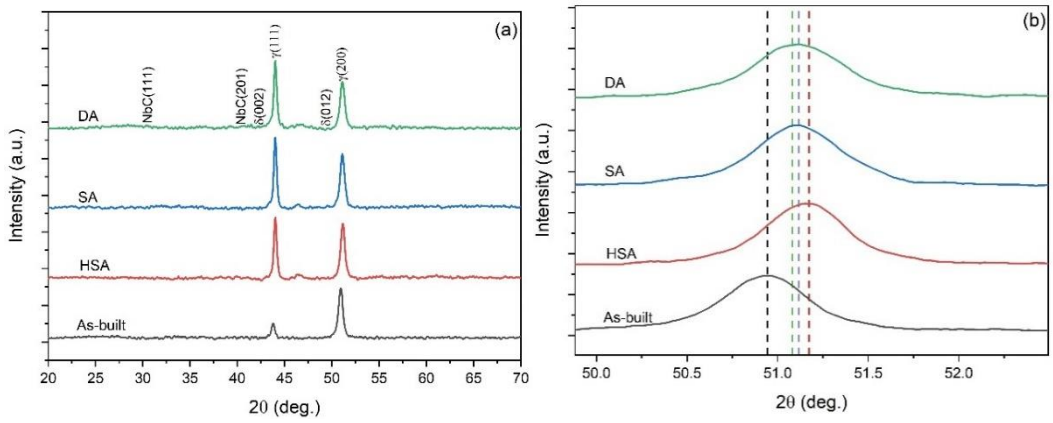

Fig. 6. (a) The XRD patterns before and after heat-treatment (b) Shifting of diffraction peaks after heat-treatment

3.4 Fracture behavior vs mechanical properties

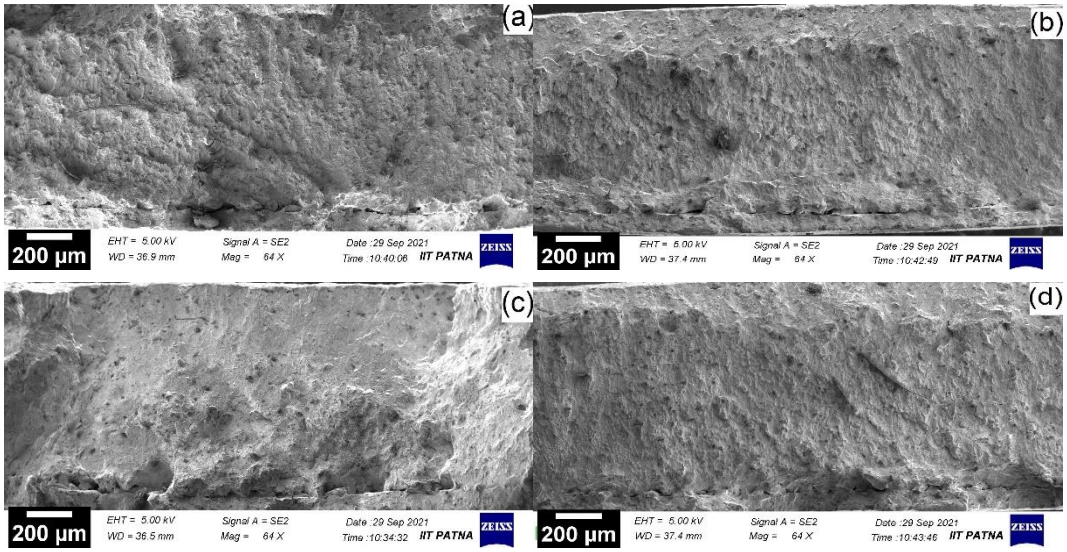

Fig. 7. Fractured surfaces of at different conditions: (a) AB, (b) HSA, (c) SA, (d), and DA

Understanding the fracture behavior during tensile tests is critical due to the orientation and heat-treatment-dependent mechanical properties. Here, as-built and heat-treated (H-built) fractured surfaces are shown in Fig. 7.

Microstructure anisotropy influences fracture mode and tensile characteristics because of the varied orientations of columnar grains with the direction of tension. Fig. 7 shows the fractured surfaces at different conditions like AB, HSA, SA, and DA. Observing Fig. 7, a shear-lip zone and a fibrous zone were found on the fractured surface of AB, but rupture of the sample HSA/SA/DA occurred at roughly 45^0 with the tensile axis on the surface of most significant shear stresses.

As seen in Fig. 7 (a), (b), (c), and (d), the micro-voids and dimples can be seen on the surface. With the availability of dimples on the fractured surface, it is evident that these dimples and micro-voids may act as favourable sites for micro-crack initiation and fracture propagation along the interdendritic regions. It is worth noting that the partially dissolved Laves phase by SA treatment results in the precipitation of a very tiny acicular δ phase. Fig. 7 (c) shows that most micro voids in the fracture profile of SA samples begin with an irregular form. To achieve the desired blend of strength and ductility with DMLS IN718, the Laves phase must first be dissolved to precipitate a small-sized δ phase at the grain boundaries by homogenizing the microstructure.

3.5 Sample orientation and heat treatment dependent microstructural evolution and strength

Young's modulus (Fig. 4d), showing the fabricated DMLS IN718 alloy. From a crystallographic standpoint, IN718 is somewhat isotropic. However, YS, UTS, and elongation depend on the build direction. The V-built sample exhibits lower YS and UTS than the H-built and D-built samples, while the elongation exhibits a reverse nature. This is possibly due to the orientation-dependent anisotropy behaviour of the material [15]. But performing the heat-treatment significantly improved the strength.

The goal of heat treatment, as previously stated, it is used to homogenize or produced improved microstructure and to improve its mechanical qualities. Because Nb segregation and Laves precipitation are limited relative to solidification during casting, Nb supersaturation in the matrix is predicted at the high cooling rates characteristic of the DMLS process [25]. In the primary γ" strengthening phase, Nb precipitates in γ matrix throughout ageing. The quantity of Nb accessible in the γ matrix, however, is also affected by the HSA/SA process. This either dissolves the Laves phase, consuming Nb, or precipitates the δ phase, consuming Nb. Because of the low temperature in direct ageing treatment, the Laves, do not allow Nb to be freed. The partially dissolved Laves phase can give some Nb after treatment at 960 ^{0}C, but it consumes more Nb to precipitate the δ phase. As a result, the quantity of

Nb accessible to precipitate γ″ is unlikely to be greater than under DA cases. When the homogenization temperature is raised to 1080 ^{0}C, all the Laves phases dissolve almost entirely, and Nb is uniformly redistributed into the gamma matrix. This increases the amount of Nb accessible for precipitation γ″ in subsequent ageing treatments compared to HSA and SA conditions. Some Nb is consumed during HSA treatment, precipitated δ phase at the grain boundaries.

4. Conclusions

This study studied the mechanical, and microstructural properties of IN718 alloy examined, considering the industrial standard heat-treatment effects. The major findings of the present study are as follows:

- The strength of the material increases significantly after heat treatment, whereas the ductility diminishes. Mechanical characteristics are less dependent on sample orientation following heat treatment.
- There is nearly 31.32% improvement in the tensile properties compared to 0^0 AB and 0^0 HT-DA samples. Compared to the horizontally and diagonally built samples, the V-built Inconel 718 has lower tensile strength but higher ductility. Anisotropy and dislocations in the samples are primarily responsible for the orientation dependency of mechanical characteristics of the as-manufactured IN718 alloy.
- The laves phase under as-built SA, and DA conditions provide favourable sites for the formation of micro-voids and the propagation of cracks. In the SA state, the extremely tiny needle-shaped δ-phase is not always harmful to ductility, while the large δ-phase under the HSA condition is prone to cracking and forms large voids for the crack to spread more.
- The XRD patterns indicated the γ, δ-phases formed during heat-treatment and showed the lateral shift of the diffraction peak is evidence of the dissolving process of the precipitate created during printing.

Acknowledgments

Sample fabrication was done at the central tool room in Bhubaneswar, heat-treatment at NIT and BIT Patna, tensile testing at NIT Patna, and SEM tests at IIT Patna, XRD at AKU Patna.

Authors' Contributions

Ajay Kumar Maurya: Conceptualization, Methodology, Investigation, Testing, Writing an original draft. **Amit Kumar:** Conceptualization, Methodology, Resources, Supervision, Writing, review, and editing.

Competing Interests

The authors declare that they have no known competing financial interests

References

[1] Frazier WE. Metal additive manufacturing: A review. J Mater Eng Perform 2014;23:1917–28. https://doi.org/10.1007/s11665-014-0958-z.

[2] Vafadar A, Guzzomi F, Rassau A, Hayward K. Advances in metal additive manufacturing: A review of common processes, industrial applications, and current challenges. Appl Sci 2021;11:1–33. https://doi.org/10.3390/app11031213.

[3] Chamanfar A, Sarrat L, Jahazi M, Asadi M, Weck A, Koul AK. Microstructural characteristics of forged and heat treated Inconel-718 disks. Mater Des 2013;52:791–800. https://doi.org/10.1016/j.matdes.2013.06.004.

[4] Chang SH, Lee SC, Huang KT, Liang C. Effects of solid-solution treatment on microstructure and mechanical properties of HIP treated alloy 718. Appl Mech Mater 2012;117–119:1315–8. https://doi.org/10.4028/www.scientific.net/AMM.117-119.1315.

[5] Dinda GP, Dasgupta AK, Mazumder J. Texture control during laser deposition of nickel-based superalloy. Scr Mater 2012;67:503–6. https://doi.org/10.1016/j.scriptamat.2012.06.014.

[6] Dinda GP, Dasgupta AK, Mazumder J. Laser aided direct metal deposition of Inconel 625 superalloy: Microstructural evolution and thermal stability. Mater Sci Eng A 2009;509:98–104. https://doi.org/10.1016/j.msea.2009.01.009.

[7] Zhu L, Xu ZF, Liu P, Gu YF. Effect of processing parameters on microstructure of laser solid forming Inconel 718 superalloy. Opt Laser Technol 2018;98:409–15. https://doi.org/10.1016/j.optlastec.2017.08.027.

[8] Chen B, Mazumder J. Role of process parameters during additive manufacturing by direct metal deposition of Inconel 718. Rapid Prototyp J 2017;23:919–29. https://doi.org/10.1108/RPJ-05-2016-0071.

[9] Huang X, Chaturvedi MC, Richards NL. Effect of homogenization heat treatment on the microstructure and heat-affected zone microfissuring in welded cast alloy 718. Metall Mater Trans A Phys Metall Mater Sci 1996;27:785–90. https://doi.org/10.1007/BF02648966.

[10] Trosch T, Strößner J, Völkl R, Glatzel U. Microstructure and mechanical properties of selective laser melted Inconel 718 compared to forging and casting. Mater Lett 2016;164:428–31. https://doi.org/10.1016/j.matlet.2015.10.136.

[11] Ni M, Liu S, Chen C, Li R, Zhang X, Zhou K. Effect of heat treatment on the microstructural evolution of a precipitation-

hardened superalloy produced by selective laser melting. Mater Sci Eng A 2019;748:275–85. https://doi.org/10.1016/j.msea.2019.01.109.

[12] Wang Z, Guan K, Gao M, Li X, Chen X, Zeng X. The microstructure and mechanical properties of deposited-IN718 by selective laser melting. J Alloys Compd 2012;513:518–23. https://doi.org/10.1016/j.jallcom.2011.10.107.

[13] Strößner J, Terock M, Glatzel U. Mechanical and Microstructural Investigation of Nickel-Based Superalloy IN718 Manufactured by Selective Laser Melting (SLM). Adv Eng Mater 2015;17:1099–105. https://doi.org/10.1002/adem.201500158.

[14] Chlebus E, Gruber K, Kuźnicka B, Kurzac J, Kurzynowski T. Effect of heat treatment on the microstructure and mechanical properties of Inconel 718 processed by selective laser melting. Mater Sci Eng A 2015;639:647–55. https://doi.org/10.1016/j.msea.2015.05.035.

[15] Maurya AK, Kumar A. Study of Microstructure and Mechanical Properties of As-built and Heat-treated Additive Manufactured Inconel 718 Alloy. ASEAN J Sci Technol Dev 2021;38. https://doi.org/10.29037/ajstd.724.

[16] Sun SH, Koizumi Y, Saito T, Yamanaka K, Li YP, Cui Y, et al. Electron beam additive manufacturing of Inconel 718 alloy rods: Impact of build direction on microstructure and high-temperature tensile properties. Addit Manuf 2018;23:457–70. https://doi.org/10.1016/j.addma.2018.08.017.

[17] Sun SH, Koizumi Y, Kurosu S, Li YP, Matsumoto H, Chiba A. Build direction dependence of microstructure and high-temperature tensile property of Co-Cr-Mo alloy fabricated by electron beam melting. Acta Mater 2014;64:154–68. https://doi.org/10.1016/j.actamat.2013.10.017.

[18] Smith DH, Bicknell J, Jorgensen L, Patterson BM, Cordes NL, Tsukrov I, et al. Microstructure and mechanical behavior of direct metal laser sintered Inconel alloy 718. Mater Charact 2016;113:1–9. https://doi.org/10.1016/j.matchar.2016.01.003.

[19] B KNAA, B SMGA, B LEMA, B EMA, B PWSA, B JHA, et al. Microstructures and mechanical behavior of Inconel 718 fabricated by selective laser melting. Acta Mater 2012;60:2229–39.

[20] Deng D, Peng RL, Brodin H, Moverare J. Microstructure and mechanical properties of Inconel 718 produced by selective laser melting: Sample orientation dependence and effects of post heat treatments. Mater Sci Eng A 2018;713:294–306. https://doi.org/10.1016/j.msea.2017.12.043.

[21] Schirra JJ, Caless RH, Hatala RW. The Effect of Laves Phase on the Mechanical Properties of Wrought and Cast + HIP Inconel 718 2012:375–88. https://doi.org/10.7449/1991/superalloys_1991_375_388.

[22] Kirka MM, Unocic KA, Raghavan N, Medina F, Dehoff RR, Babu SS. Microstructure Development in Electron Beam-Melted Inconel 718 and Associated Tensile Properties. Jom 2016;68:1012–20. https://doi.org/10.1007/s11837-016-1812-6.

[23] INCONEL® alloy 617 specifications, Special Metals n.d.:1–12.

[24] Qi H, Azer M, Ritter A. Studies of standard heat treatment effects on microstructure and mechanical properties of laser net shape manufactured INCONEL 718. Metall Mater Trans A Phys Metall Mater Sci 2009;40:2410–22. https://doi.org/10.1007/s11661-009-9949-3.

[25] Antonsson T, Fredriksson H. The effect of cooling rate on the solidification of INCONEL 718. Metall Mater Trans B Process Metall Mater Process Sci 2005;36:85–96. https://doi.org/10.1007/s11663-005-0009-0.